

Thermal Hall conductivity of electron-doped cuprates: Electrons and phonons

Marie-Eve Boulanger,^{1,*} Lu Chen,^{1,*} Vincent Oliviero,² David Vignolles,² Gaël Grissonnanche,^{1,3,4}
Kejun Xu,^{5,6,7} Zhi-Xun Shen,^{5,6,7} Cyril Proust,^{2,4} Jordan Baglo,^{1,†} and Louis Taillefer^{1,4,8,‡}

¹*Institut quantique, Département de physique & RQMP,
Université de Sherbrooke, Sherbrooke, Québec, Canada*

²*LNCMI-EMFL, CNRS UPR3228, Univ. Grenoble Alpes,
Univ. Toulouse, INSA-T, Grenoble and Toulouse, France*

³*Laboratoire des Solides Irradiés, CEA/DRF/IRAMIS, CNRS,
École Polytechnique, Institut Polytechnique de Paris, 91128 Palaiseau, France*

⁴*IRL Frontières Quantiques, Université de Sherbrooke–CNRS, Sherbrooke, Québec, Canada*

⁵*Geballe Laboratory for Advanced Materials, Stanford University, Stanford, California, USA*

⁶*Stanford Institute for Materials and Energy Sciences,*

SLAC National Accelerator Laboratory, Menlo Park, California, USA

⁷*Departments of Physics and Applied Physics, Stanford University, Stanford, California, USA*

⁸*Canadian Institute for Advanced Research, Toronto, Ontario, Canada*

(Dated: October 21, 2025)

It has recently become clear that phonons generate a sizable thermal Hall effect in cuprates, whether they are undoped, electron-doped or hole-doped (inside the pseudogap phase). At higher doping, where cuprates are reasonably good metals, mobile electrons also generate a thermal Hall effect, the thermal equivalent of the standard electrical Hall effect. Here we show that in the cleanest crystals of the electron-doped cuprate $\text{Nd}_{2-x}\text{Ce}_x\text{CuO}_4$, at high doping, the phonon and electron contributions to the thermal Hall conductivity κ_{xy} are of comparable magnitude, but of opposite sign. In samples of lower quality, phonons dominate κ_{xy} , resulting in a negative κ_{xy} at all temperatures. The fact that the negative phononic κ_{xy} in the metallic state is similar in magnitude and temperature dependence to that found in the insulating state at lower doping rules out any mechanism based on skew scattering of phonons off charged impurities, since a local charge should be screened in the metallic regime. The phononic κ_{xy} is found to persist over the entire doping range where antiferromagnetic correlations are known to be significant, suggesting that such correlations may play a role in generating the phonon thermal Hall effect in electron-doped cuprates. If the same mechanism is also at play in hole-doped cuprates, the presence of a phononic κ_{xy} below (and only below) the critical doping p^* would be evidence that spin correlations are a property of the pseudogap phase.

I. INTRODUCTION

The discovery of a large negative thermal Hall conductivity κ_{xy} in hole-doped cuprates [1], persisting down to zero doping ($p = 0$), in the Mott insulating phase [2], revealed a fascinating facet of cuprate high- T_c superconductors. This negative κ_{xy} , now attributed to phonons [2, 3], is a new experimental signature of the enigmatic pseudogap phase of cuprates, as it disappears above the critical doping p^* that marks the end of that phase. However, the microscopic mechanism that makes phonons in cuprates acquire a handedness in a magnetic field remains unknown. A number of theoretical proposals have been made, including a coupling of phonons to magnons [4] or spinons [5, 6], to collective fluctuations [7], and to a state of loop-current order with the appropriate symmetries [8], or the scattering of phonons by impurities or defects [9–13]. It is still unclear which of these mechanisms, if any, is appropriate for cuprates.

A recent study of electron-doped cuprates [14] showed that the negative thermal Hall conductivity in cuprates is also present on the other side of the phase diagram. As a function of doping, the negative κ_{xy} signal is observed from the insulating antiferromagnetic phase at $x = 0$ all the way up to $x = 0.17$, in the metallic phase above optimal doping. And here also, this negative κ_{xy} was shown to be carried by phonons.

In the metallic phase, electrons are also expected to generate a thermal Hall signal due to the Lorentz force. In this study, we show that in our cleanest crystals of the electron-doped cuprate $\text{Nd}_{2-x}\text{Ce}_x\text{CuO}_4$ (NCCO), electrons and phonons make comparable contributions to the thermal Hall conductivity in the metallic state at high doping, but with opposite sign. The electronic contribution is positive, as expected from the Wiedemann-Franz law and the known electrical Hall conductivity σ_{xy} . The negative phononic contribution is similar in magnitude and temperature dependence to that found at lower doping [14]. This shows that the phonon thermal Hall conductivity of cuprates is independent of whether the host material is an insulator or a metal. This rules out any mechanism based on the skew scattering of phonons off charged impurities, such as oxygen vacancies, as these local charges should be screened very effectively by mobile

* M.-E. B. and L. C. contributed equally to this work.

† E-mail: jordan.baglo@usherbrooke.ca

‡ E-mail: louis.taillefer@usherbrooke.ca

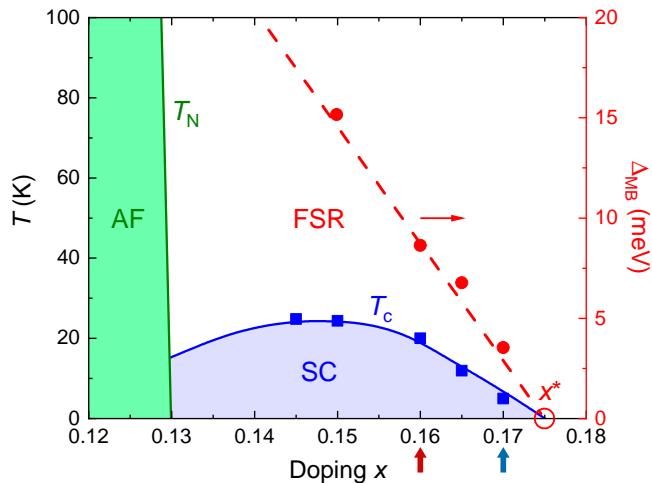


FIG. 1. Temperature-doping phase diagram of the electron-doped cuprate NCCO. The antiferromagnetic phase (AF) is bounded by the Néel temperature T_N (solid green line) and the superconducting phase (SC) by the zero-field critical temperature T_c (blue squares) [15]. The magnetic breakdown gap Δ_{MB} (red circles), obtained in a prior study from quantum oscillations, is a measure of how strongly the Fermi surface of NCCO is reconstructed [15]. The doping dependence of Δ_{MB} yields a critical doping $x^* = 0.175$ (open red circle) above which the Fermi surface is not reconstructed. The solid blue line and red dashed line are guides to the eye. In our study, we investigated two samples of NCCO with nominal concentration $x = 0.16$ (red arrow) and one with $x = 0.17$ (blue arrow).

electrons in a highly conductive metallic state.

To further characterize our samples, we sought to measure quantum oscillations. The presence of low-frequency oscillations in our cleanest sample with $x = 0.16$ shows that the Fermi surface is reconstructed at that doping, clear evidence for the presence of significant antiferromagnetic correlations even at such high doping. We speculate that these correlations may play a role in generating the phonon thermal Hall signal in electron-doped cuprates, and possibly also in the pseudogap phase of hole-doped cuprates.

II. METHODS

A. Samples

Single crystals of $\text{Nd}_{2-x}\text{Ce}_x\text{CuO}_4$ with nominal concentrations $x = 0.16$ (two samples) and $x = 0.17$ (one sample) were grown by the traveling-solvent floating-zone method in O_2 and annealed in flowing argon for 48 hours at 900°C . The three samples have a doping such that they lie in the superconducting/metallic regime of the phase diagram (see Fig. 1). The superconducting transition temperature in zero field, defined by the onset of the drop in magnetization, is $T_c = 23.5\text{K}$ and

20.0K for $x = 0.16$ and 0.17 , respectively. For the transport measurements, crystals were cut into rectangular platelets with dimensions (length between contacts \times width \times thickness, in μm) $620 \times 660 \times 90$ ($x = 0.16$, sample 1), $1114 \times 1080 \times 185$ ($x = 0.16$, sample 2), and $1000 \times 1050 \times 80$ ($x = 0.17$). Contacts were made using silver epoxy, diffused at 500°C under oxygen for 1 hour. From the same mother crystals, another pair of NCCO samples were prepared, with $x = 0.16$ and $x = 0.17$, for the tunnel diode oscillator measurements (see Section II C). The dimensions of these samples (in μm) are $730 \times 220 \times 100$ ($x = 0.16$) and $440 \times 300 \times 50$ ($x = 0.17$).

Note that it is difficult to achieve good enough electrical contacts on NCCO crystals to perform a measurement of the in-plane electrical resistivity ρ_a that is free of c -axis current contamination in this highly 2D material. For this reason, we have turned to measurements of the thermal conductivity κ_{xx} down to very low temperature (50mK) to access the residual resistivity ρ_0 of our samples via the Wiedemann-Franz (WF) law, $\kappa_0/T = L_0/\rho_0$, with $L_0 \equiv (\pi/3)(k_B/e)^2$. Heat transport does not suffer from c -axis contamination.

B. Thermal transport measurements

The thermal conductivity κ_{xx} is measured by applying a heat current J_x along the x axis of the sample (longest direction), which generates a longitudinal temperature difference $\Delta T_x = T^+ - T^-$. The thermal conductivity κ_{xx} is given by

$$\kappa_{xx} = \frac{J_x}{\Delta T_x} \left(\frac{L}{wt} \right), \quad (1)$$

where w is the sample width, t its thickness, and L the distance between T^+ and T^- . When a magnetic field is applied perpendicular to the heat current ($H \perp J_x$) (i.e., parallel to z), a transverse temperature difference ΔT_y can develop along the y axis. The thermal Hall conductivity κ_{xy} is then given by

$$\kappa_{xy} = -\kappa_{yx} \left(\frac{\Delta T_y}{\Delta T_x} \right) \left(\frac{L}{w} \right) \quad (2)$$

after antisymmetrization, i.e., $\Delta T_y(H) = [\Delta T_y(T, +H) - \Delta T_y(T, -H)]/2$. Since NCCO is a tetragonal system, we can take $\kappa_{yy} = \kappa_{xx}$. The error bar on κ_{xx} and κ_{xy} is roughly $\pm 15\%$ for each, coming mostly from the uncertainty on sample dimensions and geometric factors. The magnetic field was applied perpendicular to the CuO_2 planes. A field of $H = 15\text{T}$ is large enough to suppress superconductivity down to $T \rightarrow 0$ in all samples [16].

We use a steady-state method to measure both thermal conductivity κ_{xx} and thermal Hall conductivity κ_{xy} . The data are taken while changing temperature in discrete steps at a fixed magnetic field. The thermal gradient along the sample is provided by a resistive heater

connected to one end of the sample. The other end of the sample is glued to a copper block with silver paint which acts as a heat sink. Below 3 K, the longitudinal temperature difference ΔT_x is measured in a dilution refrigerator down to 50 mK, using two RuO₂ thermometers calibrated *in situ* as a function of temperature and magnetic field. The transverse temperature difference ΔT_y is measured using two RuO₂ thermometers connected to opposite sides of the sample. Above 3 K, ΔT_x and ΔT_y are measured in a standard variable temperature insert (VTI) system up to 100 K, using type-E thermocouples, known to have a weak magnetic field dependence. More details of the technique can be found in Refs. 2, 3, 17, and 18.

C. TDO measurements

Quantum oscillations were detected using a tunnel diode oscillator (TDO) method in a magnetic field up to 85 T down to 1.8 K. The sample is placed on a compensated spiral coil of a self-resonating LC circuit operating around 20 MHz. The circuit is driven by a tunnel diode polarized in its negative resistance region of the current-voltage characteristic. The driving system (tunnel diode + tank capacitor) is separated from the TDO coil by a 1.25-meter-long coaxial cable and the magnetic field was applied perpendicular to the CuO₂ planes.

In a TDO measurement, variations in the electrical resistance of the sample change the coil inductance through skin depth [19] resulting in a shift in the TDO resonance frequency. By measuring this shift, one can detect Shubnikov-de Haas oscillations.

III. RESULTS

A. Thermal transport

In Fig. 2(a), we display the thermal Hall conductivity of our two main samples, $x = 0.16$ (sample 1) and $x = 0.17$, plotted as κ_{xy}/H vs T below 100 K (down to 3 K), for three different magnetic fields H . At $H = 15$ T, we find that κ_{xy} is negative at all temperatures for the sample with $x = 0.17$ (blue squares), whereas it is positive at all temperatures for the sample with $x = 0.16$. The negative κ_{xy} is similar to that found at lower doping [14], down to $x = 0$, and it is due to phonons. The positive κ_{xy} is due to electrons, as we show below.

There is a contribution of phonons and electrons in both samples, but the electronic contribution is much larger in the sample with $x = 0.16$. This is confirmed by performing measurements down to very low temperature. In Fig. 3(b), we report our κ_{xy} data at $H = 15$ T taken below 4 K, plotted as κ_{xy}/T vs T . The fact that κ_{xy}/T is constant below 4 K shows that it is entirely coming from transport by fermions, i.e., electrons. Indeed, the contribution of phonons to κ_{xy} in cuprates is

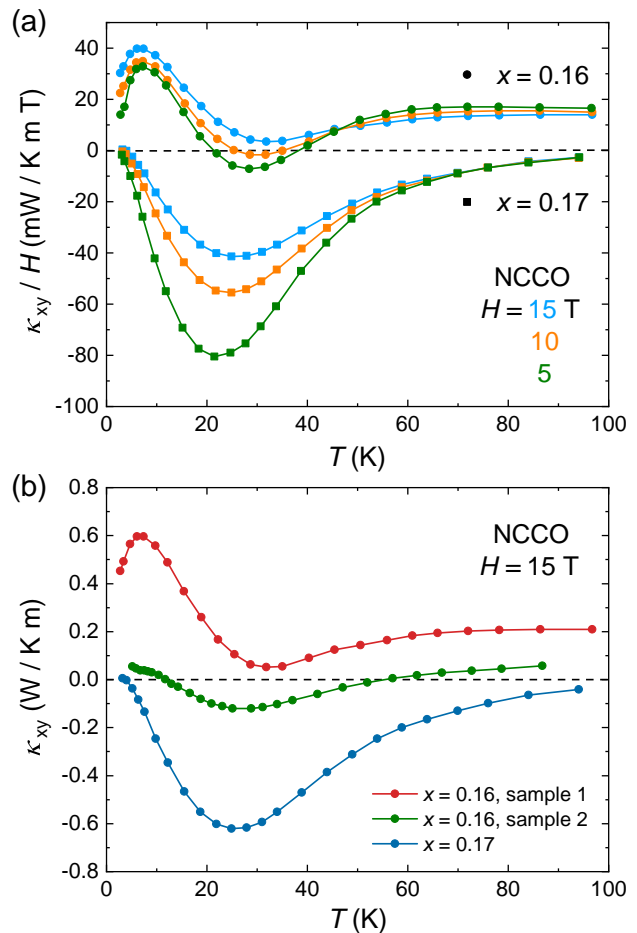


FIG. 2. (a) Temperature dependence of the thermal Hall conductivity for NCCO $x = 0.16$, sample 1 (circles) and $x = 0.17$ (squares), plotted as κ_{xy}/H vs T for fields $H = 5$ T (green), 10 T (orange), and 15 T (blue). We observe two behaviors: the negative thermal Hall conductivity of phonons (very clear in the sample with $x = 0.17$ and also visible in the sample with $x = 0.16$) and the positive thermal Hall conductivity of electrons (visible only in the sample with $x = 0.16$). (b) Thermal Hall conductivity of our three NCCO samples at $H = 15$ T, plotted as κ_{xy} vs T . At $x = 0.16$, sample 1 is cleaner than sample 2, resulting in a larger positive electronic contribution in the former.

negligible below 4 K [2]. We see that this (positive) electronic contribution is 10 times larger in the sample with $x = 0.16$, as reflected in the residual linear term obtained by extrapolating κ_{xy}/T to $T = 0$ (dashed lines), namely $\kappa_{xy}^0/T = 175 \pm 30$ mW/K²m for $x = 0.16$ and 17.5 ± 10 mW/K²m for $x = 0.17$ (Fig. 3(b)).

The thermal Hall conductivity was also measured in NCCO $x = 0.16$ sample 2, which is dirtier than sample 1. In Fig. 2(b), we see that the overall κ_{xy} signal is more negative in sample 2 compared to sample 1, which indicates that the positive electronic contribution is larger in a cleaner sample due to less scattering of electrons by impurities.

We attribute the larger positive electronic contribution

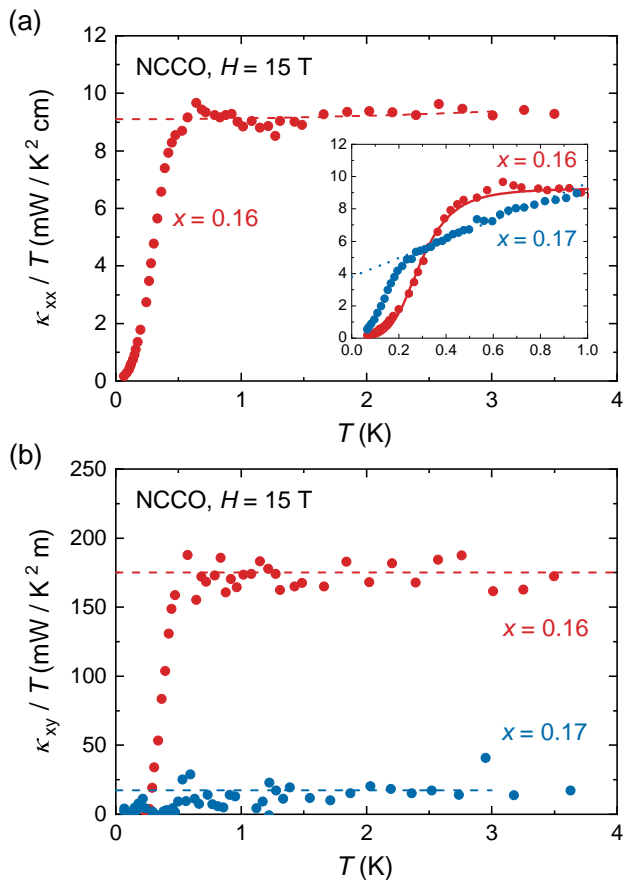


FIG. 3. (a) Thermal conductivity of NCCO $x = 0.16$ (sample 1; red dots) at $H = 15$ T, plotted as κ_{xx}/T vs T . The dashed line is a linear fit to extract the residual term in the form $\kappa_{xx}/T = \beta T^2 + \kappa_0/T$, with $\beta = 0.03$ mW/K⁴cm and $\kappa_{xx}^0/T = 9.1 \pm 0.1$ mW/K²cm. Inset: Thermal conductivity for NCCO $x = 0.16$ (red) and $x = 0.17$ (blue) at $H = 15$ T, plotted as κ_{xx}/T vs T , below 1 K. In both samples, we observe a downturn in κ_{xx}/T as $T \rightarrow 0$, characteristic of electron-phonon decoupling [20]. The red solid line is a fit of the $x = 0.16$ data to Eq. 3, which gives a decoupling temperature of $T_{\text{dec}} = 290$ mK. The blue dotted line is a linear fit to the $x = 0.17$ data that gives a residual linear term of $\kappa_{xx}^0/T = 4.0 \pm 0.1$ mW/K²cm for the $x = 0.17$ sample. (b) Thermal Hall conductivity of NCCO for $x = 0.16$ (sample 1) and $x = 0.17$ at $H = 15$ T plotted as κ_{xy}/T vs T . We extract a residual linear term of $\kappa_{xy}^0/T = 175 \pm 20$ mW/K²m for $x = 0.16$ and $\kappa_{xy}^0/T = 17.5 \pm 10$ mW/K²m for $x = 0.17$ (dashed lines).

of κ_{xy} in $x = 0.16$ sample 1 to the fact that this sample is cleaner than the $x = 0.17$ sample. This can be verified by making a direct comparison of their thermal conductivity data as $T \rightarrow 0$. Figure 3(a) shows the longitudinal thermal conductivity, plotted as κ_{xx}/T vs T , at low temperature down to $T \rightarrow 0$. Since both samples are in the metallic region of the phase diagram, a residual linear term is expected. By applying a linear fit, we obtain $\kappa_0/T = 9.1$ mW/K²cm for $x = 0.16$ and $\kappa_0/T = 4.0$ mW/K²cm for $x = 0.17$ (Fig. 3(a), main

panel, dashed line). Using the Wiedemann-Franz (WF) law, we get $\rho_0 = 2.7 \pm 0.1 \mu\Omega$ cm for the former and $\rho_0 = 6.1 \pm 0.1 \mu\Omega$ cm for the latter; there is roughly a factor of 2.3 between the two values of ρ_0 , which clearly shows that the $x = 0.16$ sample is cleaner than the $x = 0.17$ sample.

As we can observe in Fig. 3, there is a rapid downturn in both κ_{xx} and κ_{xy} below $T \sim 500$ mK. A similar downturn was observed in $\text{Pr}_{2-x}\text{Ce}_x\text{CuO}_4$ (PCCO) at $T \approx 300$ mK [21], which was attributed to the thermal decoupling between electrons and phonons at low temperature [20]. The decoupling temperature T_{dec} is extracted by fitting the κ_{xx}/T data to the expression

$$\kappa_{xx}/T = \alpha \frac{1}{1 + \frac{r}{1+r(T/T_{\text{dec}})^{n-1}}} + \beta T^2, \quad (3)$$

in which α , β , r , n , and T_{dec} are all fitting parameters [20]. In the inset of Fig. 3(a), the red solid line shows the thermal decoupling fit of our $x = 0.16$ data to Eq. 3, which gives a decoupling temperature of $T_{\text{dec}} = 290$ mK.

Figure 4(a) shows the thermal conductivity of NCCO at $x = 0.16$ plotted as κ_{xx}/T vs T , at $H = 15$ T for the full temperature range. The data are a combination of the low temperature data (obtained in a dilution fridge, circles) and the high temperature data (obtained in the VTI, triangles). In the same figure, we also plot an estimate of the maximal electronic contribution (dashed lines), calculated using the Wiedemann-Franz law: $\kappa_{xx}^e/T = L_0 \sigma_{xx}$ with $\sigma_{xx} = \rho_{xx}/(\rho_{xx}^2 + \rho_{xy}^2)$. For this estimate, we use the data of $\rho_{xx}(T)$ in PCCO at $x = 0.17$ published in Ref. 16, but with the calculated value of ρ_0 obtained from our thermal conductivity data. For $\rho_{xy}(T)$, we use the data of PCCO at $x = 0.17$ published in Ref. 22, with $\rho_{xy}(T) \equiv R_{\text{H}}(T)H$. Figure 4(a) gives us an idea of the relative contribution of electrons and phonons to κ_{xx} . The electronic part is equal to the green dashed line at $T \rightarrow 0$ and less than that at $T > 0$. The phonon part is at least as large as the distance between the red curve and the green dashed line.

In Figure 4(b), we provide an estimate of the electronic thermal Hall conductivity, κ_{xy}^e , at $x = 0.16$ (for sample 1), plotted as κ_{xy}^e/T vs T , for $H = 15$ T. The red dots at low temperature are the raw data in Fig. 3(b), and they are essentially equal to κ_{xy}^e/T since phonons contribute very little below 4 K [2]. For $T > 4$ K, our estimate of κ_{xy}^e/T is the red curve, obtained as the difference between the raw data for $x = 0.16$ (sample 1; Fig. 2(b), red dots) and the raw data for $x = 0.17$ (Fig. 2(b), blue dots). This assumes that κ_{xy} in the $x = 0.17$ sample is entirely phononic and that the two samples have the same phonon contribution. The first assumption is reasonable given that κ_{xy}^e is 10 times smaller in the $x = 0.17$ sample than in the $x = 0.16$ sample no. 1 (Fig. 3(b)). The second assumption is not unreasonable given the data for the $x = 0.16$ sample no. 2 in Fig. 2(b), which lie between the other two curves. This is what you would expect for a constant negative phonon background to which an increasing positive electronic term is added.

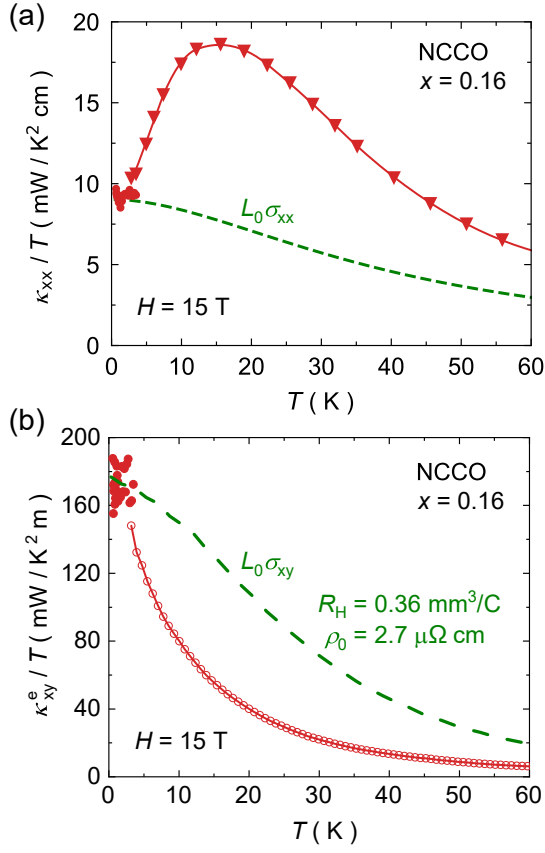


FIG. 4. (a) Thermal conductivity of NCCO at $x = 0.16$ (sample 1, red) plotted as κ_{xx}/T vs T at $H = 15$ T. The dashed green line is the electronic contribution obtained from the WF law (see text). (b) Electronic part of the thermal Hall conductivity plotted as κ_{xy}^e/T vs T for NCCO $x = 0.16$ (red) at $H = 15$ T. For $T > 4$ K, κ_{xy}^e (open red circles) is obtained by subtracting the κ_{xy} of the $x = 0.17$ sample from the $x = 0.16$ data (Fig. 2(b)), assuming the phononic κ_{xy} is the same in $x = 0.16$ and $x = 0.17$, and that the electronic contribution to the $x = 0.17$ data is negligible. The dashed green line represents an upper bound on the electronic contribution, set by $L_0\sigma_{xy}$ from the WF law. $L_0\sigma_{xy}$ is calculated by using a temperature-independent Hall coefficient R_H and temperature-dependent $\rho_{xx}(T)$ data of PCCO at $x = 0.17$ [16], but adjusted for $\rho_0 = 2.7 \mu\Omega \text{ cm}$. In order to match the value of $\kappa_{xy}^e/T = 175 \pm 20 \text{ mW/K}^2\text{m}$ at $T \rightarrow 0$, we get a Hall coefficient of $R_H = 0.36 \text{ mm}^3/\text{C}$, which is roughly half of the expected value (see text).

Let us now compare our curve for κ_{xy}^e/T (red dots and curve in Fig. 4(b)) to the electrical Hall conductivity σ_{xy} . In Fig. 4(b), we plot $L_0\sigma_{xy}$ vs T as the green dashed line, obtained from the definition $\sigma_{xy} = \rho_{xy}/(\rho_{xx}^2 + \rho_{xy}^2)$. In the $T = 0$ limit, the Wiedemann-Franz law tells us that $\kappa_{xy}^e/T = L_0\sigma_{xy}$. So we impose that equality, and thus obtain the value of $\rho_{xy} = R_H H$ at $T \rightarrow 0$, given that we know the value of ρ_{xx} at $T \rightarrow 0$, namely $\rho_0 = 2.7 \mu\Omega \text{ cm}$. We get a Hall coefficient equal to $R_H = 0.36 \text{ mm}^3/\text{C}$. This is half the value that one must get for an unreconstructed Fermi surface, namely $R_H = V/(ne) = 0.7 \text{ mm}^3/\text{C}$,

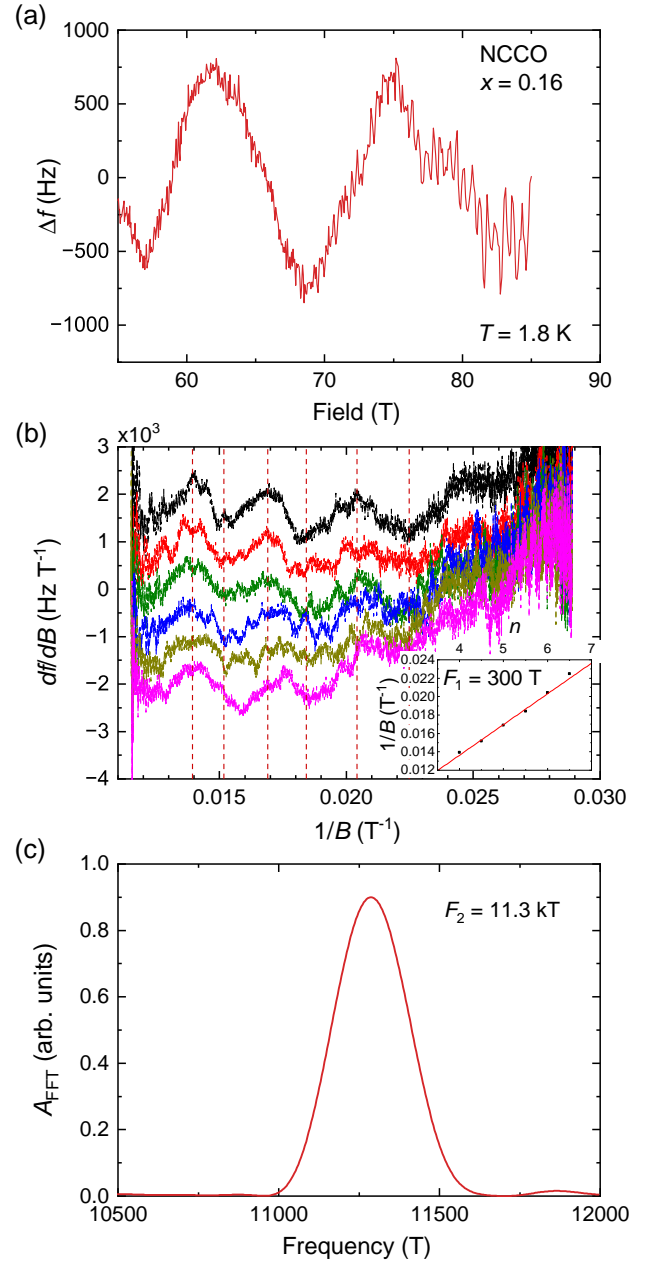


FIG. 5. Quantum oscillation pattern observed by TDO measurement. (a) The oscillatory part of the TDO signal after removing a smooth background at $T = 1.8$ K. (b) Plot of TDO signal derivative df/dB vs. $1/B$ with locations of extrema marked; traces vertically offset for visibility. Inset: $1/B$ vs. index n of extrema; slope of linear fit yields $F_1 = 300 \pm 20$ T. (c) FFT of data showing the high-frequency peak at $F_2 = 11300 \pm 100$ T.

where V is the volume per Cu atom, e is the electron charge and $n = 1 - x$ is the carrier density contained in the full Fermi surface at a doping x . The fact that we get a Hall coefficient that is lower than that reference value is consistent with the Fermi surface being reconstructed, i.e., with $x < x^*$ [22]; such Fermi-surface reconstruction

in NCCO up to x^* has been confirmed by recent ARPES work [23].

B. Quantum oscillations

Separate evidence that the NCCO $x = 0.16$ sample 1 is cleaner than the $x = 0.17$ sample comes from our quantum oscillation data. By performing TDO measurements in identical conditions for both $x = 0.16$ (sample 1) and $x = 0.17$ up to 85 T, we were able to observe quantum oscillations in the $x = 0.16$ sample but not in the $x = 0.17$ sample, which suggests that the $x = 0.16$ sample is indeed cleaner than the $x = 0.17$ sample, since the amplitude of quantum oscillations is exponentially proportional to the electronic mean free path.

The quantum oscillation data taken in the $x = 0.16$ sample (after subtracting a smooth background) are shown in Fig. 5(a). Two oscillatory components are visible: a low frequency with ~ 2 periods between 50 T and 90 T, and a high frequency clearly visible above 80 T. A determination of the lower frequency is made by locating and indexing the peaks and troughs in the derivative df/dB (Fig. 5(b)), with the slope of a linear fit to $1/B$ vs. n (inset) yielding $F_1 = 300 \pm 20$ T. The high-frequency oscillations are readily separable from signal background, and a discrete Fourier transform suffices for a reliable determination of their frequency $F_2 = 11300 \pm 100$ T (Fig. 5(c)).

Below $x^* = 0.175$ (Fig. 1), the Fermi surface of NCCO undergoes a reconstruction due to the antiferromagnetic ordering, which results in small electron-like and hole-like pockets [24]. The low frequency oscillations (F_1) come from the small hole pocket, while the high frequency (F_2) can be explained by either a remnant ‘‘gossamer’’ large Fermi surface [25] or by the magnetic breakdown between the hole- and electron-like pockets of the reconstructed Fermi surface [15, 26]. In either case, this high frequency F_2 effectively corresponds to the area of an orbit around the large unreconstructed Fermi surface. Its value is given by $F = n\Phi_0$, where the 2D carrier density is equal to $n = 1 - x$ per Cu. Given $F = 11.3$ kT, we get $x = 0.160$ if we assume that the in-plane lattice spacing has a value of 3.92 Å. This value is within the range of values quoted in the literature, namely 3.91 ± 0.01 Å [27] and 3.95 ± 0.01 Å [28]. This frequency tells us that the average radius of the roughly circular Fermi surface is given by the Onsager relation $F = \hbar k_F^2/2e$, from which we infer $k_F = 0.586 \pm 0.003$ Å $^{-1}$.

From the Lifshitz-Kosevich (LK) theory, the temperature and magnetic field dependence of the oscillation amplitude are determined by the product of the thermal damping factor R_T and the Dingle damping factor R_D , defined as

$$R_T = \frac{\alpha T m^*/m_e}{B \sinh(\alpha T m^*/m_e B)}, \quad (4)$$

$$R_D = \exp[-\alpha T_D m^*/m_e B], \quad (5)$$

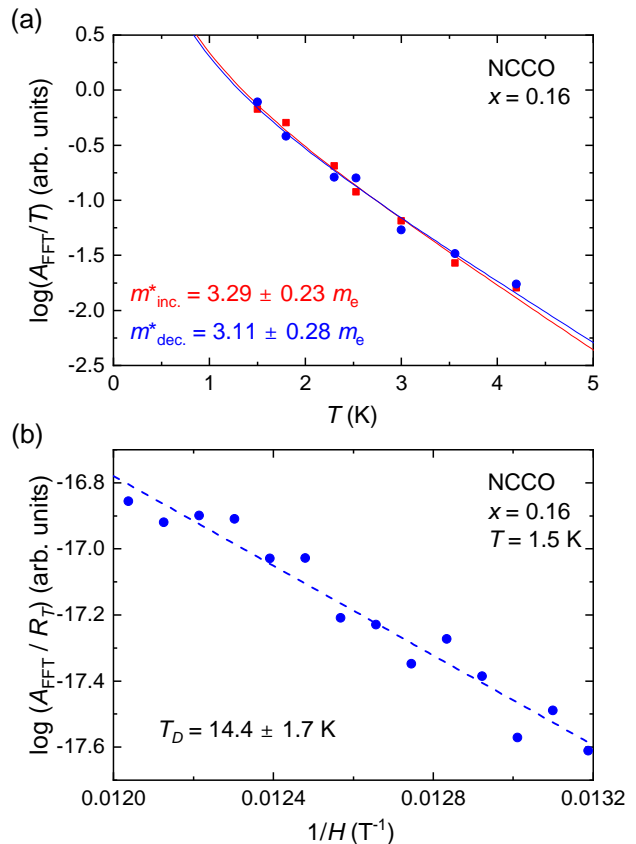


FIG. 6. (a) The temperature dependence of the FFT amplitude for the high frequency oscillation (F_2), normalized in the $T \rightarrow 0$ limit. Separate fits to Eq. 4 (solid lines) for data collected during the increasing (red) and decreasing (blue) stages of the field pulse yield effective masses of $m_{\text{inc}}^* = 3.29 \pm 0.23 m_e$ and $m_{\text{dec}}^* = 3.11 \pm 0.28 m_e$, respectively; we use $m^* = 3.20 \pm 0.18 m_e$ for subsequent analysis. (b) Dingle plot of the amplitude vs magnetic field for the same oscillation at $T = 1.5$ K, giving a Dingle temperature $T_D = 14.4 \pm 1.7$ K. The dashed line is a fit to Eq. 5.

where the Dingle temperature $T_D = \hbar/2\pi k_B \tau$, the constant $\alpha \equiv 2\pi^2 k_B m_e / e \hbar = 14.69$ T/K, τ is the scattering time, k_B is the Boltzmann constant, m^* is the effective carrier mass, and m_e is the bare electron mass. Equation 5 can also be expressed in terms of the electronic mean free path ℓ_e : $R_D = \exp[-\pi r_c / \ell_e]$, where the cyclotron radius $r_c = m^* v_F / eB$. We can then fit the temperature dependence of the normalized damping factor (Fig. 6(a)) to Eq. 4 to obtain an effective mass of $m^* = 3.20 \pm 0.18 m_e$ for the high frequency; this allows us to extract the Fermi velocity $v_F = \hbar k_F / m^* = (2.12 \pm 0.12) \times 10^5$ m/s. Figure 6(b) shows the field dependence of the oscillation amplitude. A fit to Eq. 5 yields a Dingle temperature of $T_D = 14.4 \pm 1.7$ K, corresponding to a scattering lifetime $\tau = (8.4 \pm 1.0) \times 10^{-14}$ s and a mean free path $\ell_e = v_F \tau = 178 \pm 14$ Å. Both the effective mass and the Dingle temperature extracted here are consistent with previous quantum oscillation results

on NCCO at $x = 0.15$ [26, 28].

IV. DISCUSSION

The main finding of this study is the positive thermal Hall conductivity of our NCCO $x = 0.16$ sample no. 1, compared to a large negative κ_{xy} signal in the $x = 0.17$ sample (Fig. 2(b)). Knowing from a previous study [14] that the κ_{xy} observed at $x = 0.17$ is dominated by phonons, we propose two distinct contributions to κ_{xy} in NCCO at high doping ($x > 0.15$): a positive contribution from electrons, and a negative contribution from phonons. That the electronic κ_{xy} is larger in the $x = 0.16$ sample is simply due to the fact that the $x = 0.16$ sample is cleaner (i.e., it has a longer electronic mean free path) than the $x = 0.17$ sample, as shown by the smaller residual resistivity ρ_0 of the $x = 0.16$ sample and the absence of quantum oscillations in the $x = 0.17$ sample. At fixed nominal doping ($x = 0.16$), samples of different quality exhibit different magnitude of κ_{xy}^e (Fig. 2(b)).

Combining these results with a previous study [14], we find that the large negative phonon contribution has similar magnitude and temperature dependence at all doping levels of the electron-doped cuprates NCCO and PCCO. This observation indicates that the mechanism behind the phonon thermal Hall effect in electron-doped cuprates is similar for all doping levels, regardless of whether the system is an insulator or metal. This places strong a constraint on possible mechanisms behind the phonon thermal Hall effect and rules out any mechanism based on the skew scattering of phonons off charged impurities [11], such as oxygen vacancies, as these local charges should be screened very effectively by mobile electrons in a highly conductive metallic state.

So what makes phonons chiral in cuprates? One possible explanation is the scattering of phonons by impurities embedded within an antiferromagnetic environment [13]. Both the magnitude of the extracted Hall coefficient ($R_H < 0.7 \text{ mm}^3/\text{C}$) and the presence of a low frequency in the quantum oscillation data in our NCCO $x = 0.16$ sample confirm its proximity to the Fermi surface reconstruction point x^* , with $x < x^*$, where short-range antiferromagnetic correlations are still prominent. A large negative phonon contribution, similar in magnitude and temperature dependence, persists from the antiferromagnetically ordered Mott insulating state all the way up to the metallic state close to x^* , which is consistent with a scenario of antiferromagnetic ordering playing a key role in the phonon thermal Hall effect.

It is worth noting that a similar κ_{xy} consisting of both a negative phononic contribution and a positive electronic contribution has also been observed in the hole-doped cuprate $\text{La}_{1.6-x}\text{Nd}_{0.4}\text{Sr}_x\text{CuO}_4$ at $p = 0.20$ [1], and high-field NMR measurements of the closely related $\text{La}_{2-x}\text{Sr}_x\text{CuO}_4$ have revealed the presence of an antiferromagnetic spin-glass phase from $p = 0.02$ all the way to

$p^* \approx 0.19$ [29]. The similar behavior of the phonon thermal Hall effect in hole-doped cuprates and electron-doped cuprates indicates that the same mechanism involving antiferromagnetic correlations could potentially also explain the phonon κ_{xy} in hole-doped cuprates, as has been suggested by a recent study of impurity-induced phonon thermal Hall effect in the antiferromagnetic phase of Sr_2IrO_4 [30].

V. SUMMARY

We have measured the thermal conductivity κ_{xx} and the thermal Hall conductivity κ_{xy} of the electron-doped cuprate NCCO at dopings $x = 0.16$ and $x = 0.17$. In the $x = 0.16$ sample, we observe two distinct channels for thermal Hall conductivity in the metallic state: a positive channel contributed by electrons and a negative channel contributed by phonons. The fact that the negative phononic contribution is comparable in magnitude and temperature dependence regardless of the system being an insulator (at low doping) or a metal (at high doping) indicates that its origin is unlikely to come from skew scattering of phonons off charged impurities, since such a mechanism should depend strongly on the screening from mobile electrons. The fact that the negative phonon thermal Hall effect persists from the antiferromagnetically ordered phase all the way up to x^* (Fig. 1), where short-range antiferromagnetic correlations are still present, is consistent with spin texture playing a role in the underlying mechanism for the phonon thermal Hall effect. This type of mechanism, whereby phonons are scattered by spin texture or defects embedded in a magnetic order, could also apply to hole-doped cuprates inside their pseudogap phase (below the critical doping p^*).

VI. ACKNOWLEDGMENTS

We thank S. Fortier for his assistance with the experiments, and the cryogenics team at the Institut Quantique for their support. L. T. acknowledges support from the Canadian Institute for Advanced Research (CIFAR) as a CIFAR Fellow, and funding from the Institut Quantique, the Natural Sciences and Engineering Research Council of Canada (Grant No. PIN:123817), and a Canada Research Chair. C. P. acknowledges support from the EUR grant NanoX No. ANR-17-EURE-0009 and from the ANR grant NEPTUN No. ANR-19-CE30-0019-01. G. G. acknowledges support from STeP2 No. ANR-22-EXES-0013, QuantExt No. ANR-23-CE30-0001-01, Audace CEA No. ANR-24-RRII-0004, and the École Polytechnique Foundation. Z.-X.S. acknowledges the support of the U.S. Department of Energy, Office of Science, Office of Basic Energy Sciences, Division of Material Sciences and Engineering, under contract DE-AC02-76SF00515. M.-E. B., L. C., G. G., J. B., and L. T. have benefited from their affiliation to the RQMP [31]. This

research was undertaken thanks, in part, to funding from the Canada First Research Excellence Fund. This re-

search project No. 324046 is made possible thanks to funding from the Fonds de recherche du Québec.

-
- [1] G. Grissonnanche, A. Legros, S. Badoux, É. Lefrançois, M. L. V. Zlatko, F. Laliberté, A. Gourgout, J.-S. Zhou, S. Pyon, T. Takayama, H. Takagi, S. Ono, N. Doiron-Leyraud, and L. Taillefer, Giant thermal Hall conductivity in the pseudogap phase of cuprate superconductors, *Nature* **571**, 376 (2019).
- [2] M.-E. Boulanger, G. Grissonnanche, S. Badoux, A. Alaire, É. Lefrançois, A. Legros, A. Gourgout, M. Dion, C. H. Wang, X. H. Chen, R. Liang, W. N. Hardy, D. A. Bonn, and L. Taillefer, Thermal Hall conductivity in the cuprate Mott insulators Nd_2CuO_4 and $\text{Sr}_2\text{CuO}_2\text{Cl}_2$, *Nat. Commun.* **11**, 5325 (2020).
- [3] G. Grissonnanche, S. Thériault, A. Gourgout, M.-E. Boulanger, É. Lefrançois, A. Ataei, F. Laliberté, M. Dion, J.-S. Zhou, S. Pyon, T. Takayama, H. Takagi, N. Doiron-Leyraud, and L. Taillefer, Chiral phonons in the pseudogap phase of cuprates, *Nat. Phys.* **16**, 1108 (2020).
- [4] M. Ye, L. Savary, and L. Balents, Phonon Hall viscosity in magnetic insulators (2021), arXiv:2103.04223 [cond-mat.str-el].
- [5] R. Samajdar, S. Chatterjee, S. Sachdev, and M. S. Scheurer, Thermal Hall effect in square-lattice spin liquids: A Schwinger boson mean-field study, *Phys. Rev. B* **99**, 165126 (2019).
- [6] Y. Zhang, Y. Teng, R. Samajdar, S. Sachdev, and M. S. Scheurer, Phonon Hall viscosity from phonon-spinon interactions, *Phys. Rev. B* **104**, 035103 (2021).
- [7] L. Mangeolle, L. Balents, and L. Savary, Thermal conductivity and theory of inelastic scattering of phonons by collective fluctuations, *Phys. Rev. B* **106**, 245139 (2022).
- [8] C. M. Varma, Thermal Hall effect in the pseudogap phase of cuprates, *Phys. Rev. B* **102**, 075113 (2020).
- [9] J.-Y. Chen, S. A. Kivelson, and X.-Q. Sun, Enhanced Thermal Hall Effect in Nearly Ferroelectric Insulators, *Phys. Rev. Lett.* **124**, 167601 (2020).
- [10] H. Guo and S. Sachdev, Extrinsic phonon thermal Hall transport from Hall viscosity, *Phys. Rev. B* **103**, 205115 (2021).
- [11] B. Flebus and A. H. MacDonald, Charged defects and phonon Hall effects in ionic crystals, *Phys. Rev. B* **105**, L220301 (2022).
- [12] X.-Q. Sun, J.-Y. Chen, and S. A. Kivelson, Large extrinsic phonon thermal Hall effect from resonant scattering, *Phys. Rev. B* **106**, 144111 (2022).
- [13] H. Guo, D. G. Joshi, and S. Sachdev, Resonant thermal Hall effect of phonons coupled to dynamical defects, *Proc. Natl. Acad. Sci. U.S.A.* **119**, (46) e2215141119 (2022).
- [14] M.-E. Boulanger, G. Grissonnanche, É. Lefrançois, A. Gourgout, K.-J. Xu, Z.-X. Shen, R. L. Greene, and L. Taillefer, Thermal Hall conductivity of electron-doped cuprates, *Phys. Rev. B* **105**, 115101 (2022).
- [15] T. Helm, M. V. Kartsovnik, I. Sheikin, M. Bartkowiak, F. Wolff-Fabris, N. Bittner, W. Biberacher, M. Lambacher, A. Erb, J. Wosnitza, and R. Gross, Magnetic Breakdown in the Electron-Doped Cuprate Superconductor $\text{Nd}_{2-x}\text{Ce}_x\text{CuO}_4$: The Reconstructed Fermi Surface Survives in the Strongly Overdoped Regime, *Phys. Rev. Lett.* **105**, 247002 (2010).
- [16] F. F. Tafti, F. Laliberté, M. Dion, J. Gaudet, P. Fournier, and L. Taillefer, Nernst effect in the electron-doped cuprate superconductor $\text{Pr}_{2-x}\text{Ce}_x\text{CuO}_4$: Superconducting fluctuations, upper critical field H_{c2} , and the origin of the T_c dome, *Phys. Rev. B* **90**, 024519 (2014).
- [17] G. Grissonnanche, F. Laliberté, S. Dufour-Beauséjour, M. Matusiak, S. Badoux, F. F. Tafti, B. Michon, A. Rippe, O. Cyr-Choinière, J. C. Baglo, B. J. Ramshaw, R. Liang, D. A. Bonn, W. N. Hardy, S. Krämer, D. LeBoeuf, D. Graf, N. Doiron-Leyraud, and L. Taillefer, Wiedemann-Franz law in the underdoped cuprate superconductor $\text{YBa}_2\text{Cu}_3\text{O}_y$, *Phys. Rev. B* **93**, 064513 (2016).
- [18] L. Chen, L. Le Roux, G. Grissonnanche, M.-E. Boulanger, S. Thériault, R. Liang, D. A. Bonn, W. N. Hardy, S. Pyon, T. Takayama, H. Takagi, K.-J. Xu, Z.-X. Shen, and L. Taillefer, Planar Thermal Hall Effect from Phonons in Cuprates, *Phys. Rev. X* **14**, 041011 (2024).
- [19] T. Coffey, Z. Bayindir, J. F. DeCarolis, M. Bennett, G. Esper, and C. C. Agosta, Measuring radio frequency properties of materials in pulsed magnetic fields with a tunnel diode oscillator, *Rev. Sci. Instrum.* **71**, 4600 (2000).
- [20] M. F. Smith, J. Paglione, M. B. Walker, and L. Taillefer, Origin of anomalous low-temperature downturns in the thermal conductivity of cuprates, *Phys. Rev. B* **71**, 014506 (2005).
- [21] R. W. Hill, C. Proust, L. Taillefer, P. Fournier, and R. L. Greene, Breakdown of Fermi-liquid theory in a copper-oxide superconductor, *Nature* **414**, 711 (2001).
- [22] S. Charpentier, G. Roberge, S. Godin-Proulx, X. Béchamp-Laganière, K. D. Truong, P. Fournier, and P. Rauwel, Antiferromagnetic fluctuations and the Hall effect of electron-doped cuprates: Possibility of a quantum phase transition at underdoping, *Phys. Rev. B* **81**, 104509 (2010).
- [23] J. He, C. R. Rotundu, M. S. Scheurer, Y. He, M. Hashimoto, K.-J. Xu, Y. Wang, E. W. Huang, T. Jia, S. Chen, B. Moritz, D. Lu, Y. S. Lee, T. P. Devereaux, and Z.-x. Shen, Fermi surface reconstruction in electron-doped cuprates without antiferromagnetic long-range order, *Proceedings of the National Academy of Sciences* **116**, 3449 (2019).
- [24] J. Lin and A. J. Millis, Theory of low-temperature Hall effect in electron-doped cuprates, *Phys. Rev. B* **72**, 214506 (2005).
- [25] K.-J. Xu, Q. Guo, M. Hashimoto, Z.-X. Li, S.-D. Chen, J. He, Y. He, C. Li, M. H. Berntsen, C. R. Rotundu, Y. S. Lee, T. P. Devereaux, A. Rydh, D.-H. Lu, D.-H. Lee, O. Tjernberg, and Z.-X. Shen, Bogoliubov quasiparticle on the gossamer Fermi surface in electron-doped cuprates, *Nature Physics* **19**, 1834 (2023).
- [26] T. Helm, *Electronic Properties of Electron-Doped Cuprate Superconductors Probed by High-Field Magnetotransport*, Ph.D. thesis, Technische Universität München, Munich (2013).

- [27] A. J. Schultz, J. D. Jorgensen, J. L. Peng, and R. L. Greene, Single-crystal neutron-diffraction structures of reduced and oxygenated $\text{Nd}_{2-x}\text{Ce}_x\text{CuO}_y$, *Physical Review B* **53**, 5157 (1996).
- [28] T. Helm, M. V. Kartsovnik, M. Bartkowiak, N. Bittner, M. Lambacher, A. Erb, J. Wosnitzer, and R. Gross, Evolution of the Fermi surface of the electron-doped high-temperature superconductor $\text{Nd}_{2-x}\text{Ce}_x\text{CuO}_4$ revealed by Shubnikov–de Haas oscillations, *Phys. Rev. Lett.* **103**, 157002 (2009).
- [29] M. Frachet, I. Vinograd, R. Zhou, S. Benhabib, S. Wu, H. Mayaffre, S. Krämer, S. K. Ramakrishna, A. P. Reyes, J. Debray, T. Kurosawa, N. Momono, M. Oda, S. Komiya, S. Ono, M. Horio, J. Chang, C. Proust, D. LeBoeuf, and M.-H. Julien, Hidden magnetism at the pseudogap critical point of a cuprate superconductor, *Nature Physics* **16**, 1064 (2020).
- [30] A. Ataei, G. Grissonnanche, M.-E. Boulanger, L. Chen, É. Lefrançois, V. Brouet, and L. Taillefer, Phonon chirality from impurity scattering in the antiferromagnetic phase of Sr_2IrO_4 , *Nat. Phys.* **20**, 585 (2024).
- [31] Regroupement québécois sur les matériaux de pointe (RQMP), <https://doi.org/10.69777/309032>.